J Nanopart Res (2024) 26:136
https://doi.org/10.1007/s11051-024-06048-6

RESEARCH

Effect of the AuNPs@amox system on antibiotic-resistant bacteria

Andrea-Sarahí Balderrama-González · Hilda-Amelia Piñón-Castillo · Claudia-Adriana Ramírez-Valdespino · Reyna Reyes-Martínez · Hilda-Esperanza Esparza-Ponce

Received: 28 February 2024 / Accepted: 8 June 2024 / Published online: 22 June 2024

Abstract Antibacterial resistance has been associated with significant morbidity and mortality, leading to increased costs due to prolonged hospitalization. In this study, we report the synthesis of amoxicillin-functionalized gold nanoparticles (AuNPs@amox) through the chemical reduction of [0.01 M] HAuCl4 with [0.001 M] of amoxicillin in a single step. Amoxicillin, a β-lactam antibiotic can reduce to Au^0 through the protonated amino group present in its molecular structure. Multidrug-resistant bacteria, *Staphylococcus aureus* and *Acinetobacter baumannii* were used. Both were isolated from clinical samples and were resistant to Amoxicillin, so it was chosen for functionalization to evaluate its effect on the resistant bacteria.

It was obtaining AuNPs@amox with a bimodal size of 9 ± 2 nm, smaller ones of 1 ± 0.6 nm, and amoxicillin loading of 27.5% on their surface. X-ray photoelectron spectroscopy (XPS) analysis revealed an electrostatic bond between sulfur and the amino group of the antibiotic. Colloidal stability was evaluated through zeta potential and hydrodynamic diameter in trypticase soy broth (0.5X), resulting in -14.1 mV and 138 ± 10 nm, respectively. The AuNPS@amox exhibits antibacterial properties against the resistant strains *Acinetobacter baumannii* and Methicillin-resistant *S. aureus* (MRSA), inhibiting up to 77% and 80%, respectively. Upon internalization of AuNPs@amox into the cell, it induces ruptures in the cell wall, leading to cell lysis. It also disrupted the production of biofilms at 10 µg/mL.

This work aims to contribute to developing a system that improves drug transport in resistant bacteria—generating high inhibition and significant damage to the resistance mechanisms of resistant bacteria, using very low concentrations to mitigate side effects.

Keywords Amoxicillin · Antimicrobial resistance · Biofilm generation · Efflux pumps damage · Gold nanoparticles

Supplementary Information The online version contains supplementary material available at https://doi.org/10.1007/s11051-024-06048-6.

A.-S. Balderrama-González · C.-A. Ramírez-Valdespino · H.-E. Esparza-Ponce (✉)
Centro de Investigación en Materiales Avanzados, Complejo Industrial Chihuahua, S. C. Miguel de Cervantes 120, 31109 Chihuahua, Chihuahua, México
e-mail: hilda.esparza@cimav.edu.mx

H.-A. Piñón-Castillo (✉) · R. Reyes-Martínez
Universidad Autónoma de Chihuahua Circuito No. 2, Nuevo Campus Universitario, Apdo. Postal 1552, 31240 Chihuahua, Chihuahua, México
e-mail: hpinon@uach.mx

Introduction

Antimicrobial resistance (AMR) is a natural phenomenon in bacteria. However, the overuse of antibiotics and the spread of resistant genes have led to the development of various biochemical resistance

mechanisms [1, 2]. AMR has resulted in the loss of millions of dollars and numerous deaths per year [3, 4]. Projections for 2050 suggest ten million deaths annually among patients infected by this group of bacteria [5].

Most antibiotics are designed to inhibit cell wall synthesis, DNA replication, and protein synthesis [6]. However, bacteria have adapted to evolve various biochemical mechanisms to evade these antimicrobial targets, such as the generation of biofilms, excretion of efflux pumps, changes in the permeability of their membrane, and cell wall. Resistant pathogens can destroy the drug target through enzymatic inactivation, such as β-lactamase enzymes that damage β-lactam antibiotics [7–9]. An example of such antibiotics is amoxicillin, a penicillin derivative whose primary function is to inhibit the connection between the linear peptidoglycan chains forming the bacteria cell wall [10].

Traditional antibiotics often fail to eradicate resistant bacteria, leading to an increased search for new tools. Several researchers have reported that the use of metal nanoparticles (MNPs) has gained interest due to their intrinsic properties. The antibacterial effect of MNPs is highly dependent on their physicochemical characteristics, such as size, surface area, and charge [11]. These properties can be manipulated by controlling pH, temperature, precursor concentration, and reaction time [12, 13]. The size and shape play a key role against resistant bacteria due to their surface-to-volume ratio, resulting in higher surface particle activity with the site of interest [14]. The use of MNPs in the medical field has opened up opportunities for extensive research into their antibacterial mechanisms. The degradation or inhibition of biofilm generation, interaction and penetration of the cell wall, production of reactive oxygen species (ROS), damage to efflux pumps, and interaction with metabolic pathways, DNA, and proteins are among the different antimicrobial mechanisms that have been reported for MNPs [15–17].

Gold is a metallic material that has been synthesized in different morphologies and sizes [16]. One method to synthesize gold nanoparticles (AuNPs) is colloidal chemical synthesis. Likewise, gold, being a multivalent metal, allows binding to many types of ligands, making it ideal for medical applications [17]. The chemical precipitation of gold nanoparticles also offers several advantages, such as controlling the size distribution, minimizing agglomeration and aggregation of particles, and the simplicity of the synthesis process [16].

The use of plant extract [18] or cell-free supernatant of microorganisms [19] has been employed for the synthesis of gold nanoparticles. These nanoparticles have demonstrated efficacy in inhibiting the growth of bacteria such as MRSA and *E. coli* [19], *Pseudomonas aeruginosa*, *Bacillus subtilis*, as well as fungi such as *Aspergillus niger* [20]. Gold nanoparticles' biosynthesis has also been shown to efficiently inhibit biofilm formation [21, 22], exhibit anticancer activity against HepG2 cancer cell lines [21] or adenocarcinoma cells (Mcf7-HTB-222) [22] and liver cancer cell-lines HepG2 [20], and even demonstrate antioxidant activity [22, 23].

Recently the conjugation of AuNPs with antibiotics and the trend of enhancing the antibacterial capabilities of the latter have been studied [24–33]. This approach reduces the need for high doses to mitigate the side effects that may develop in the human body when antibiotics are used. Recent studies have shown an increase in bacterial susceptibility to antibiotics such as amikacin, vancomycin, amoxicillin, and ampicillin, when conjugated with different types of nanoparticles. This positions it as a promising pathway for research against antimicrobial resistance generated by bacteria [34–37].

Such was the case of Mohamed 2020, when synthesizing AuNPs with a size of 8 nm loaded with ampicillin and amoxicillin they found a potential antibacterial agent against resistant pathogens with low cytotoxicity [32]. Rocca et. al., demonstrated a reduction of biofilm formation up to 70% in Gram-negative bacteria and 60% in Gram-positive bacteria using amoxicillin-conjugated AuNPs with short periods of irradiations [38].

On the other hand, Hasoon et. al., biosynthesized ciprofloxacin-conjugated AuNPs with sizes below 20 nm. These were shown to have a more pronounced inhibitory effect on *K. pneumoniae* and *S. pneumoniae* clinical isolates compared to ciprofloxacin or AuNPs alone, causing significant damage to biofilm formation [39].

Giráldez-Pérez et. al., have succeeded in developing AuNPs nanocomplexes from amoxicillin, using a deoxyribonucleic acid (DNA) biopolymer as a functionalization medium with an average size of 3 nm. In this study, they generated a synergy between

AuNPs and amoxicillin, causing a response to oxidative stress and interaction with the cell membrane and enhancing the antimicrobial capacity of amoxicillin and AuNPs compared with their free form [40].

In the research conducted by Halawani et. al., they used *Juniperus excelsa* extract for the biosynthesis of AuNPs by conjugating them with amoxicillin and sodium tripolyphosphate to anchor the antibiotic to the surfaces of the nanoparticles and obtaining an approximate size of 24 nm. They report an increase in the inhibition of resistant strains by 83 times at low concentrations against MRSA and *E. coli*, with an antibiotic release of 90% after 3 days [19].

Finally, Jawad et. al., managed to biosynthesize AuNPs functionalized with amikacin against *P. aeruginosa* and *S. pneumoniae*, obtaining significant differences compared to the control. They also achieved a considerable reduction in biofilm formation and demonstrated potent antioxidant activity [41].

Smaller particles between 2 and 10 nm generally correlate with greater antibacterial effects [42], due to their large contact surface area with bacterial cells. The objective of the research was the synthesis of amoxicillin-functionalized gold nanoparticles (AuNPs@amox), which was conducted with amoxicillin serving as both a reducing and stabilizing agent for the AuNPs. The antibiotic was confirmed by XPS; the study also evaluated the effects and antimicrobial properties of AuNPs@amox, characterized by a bimodal size distribution of less than 10 nm. The investigation included assessments of damage to biofilm production and efflux pumps against Methicillin-resistant *S. aureus* (MRSA) and multidrug-resistant *A. baumannii.*

Materials and methods

Synthesis of gold nanoparticles functionalized with amoxicillin

The synthesis of AuNPs coated with amoxicillin (AuNPs@amox) was modified by adjusting the reaction time and temperature based on the protocol described by Demurtas et al. [43], with a molar ratio 4:1 for AuNPs and amoxicillin. Deionized water (57.9 mL) in a temperature-controlled bath was heated to a temperature of 45 °C. Subsequently, 600 µL of $HAuCl_4$ solution [0.01 M] was added drop by drop, while simultaneously introducing 1500 µL of the amoxicillin solution [0.001 M]. The mixture was allowed to blend under magnetic agitation for 5 min. Following this, the reaction was left to stir for 2 h or until a subtle purple emerged, maintaining a stirring speed of 100 rpm at 45 °C.

Synthesis of gold nanoparticles control

The synthesis of AuNPs was modified by adjusting the reaction time and temperature according to the protocol described by Silvero et al., [29]. AuNPs were prepared using a chemical reduction method with $NaBH_4$. The synthesis was conducted in a water bath at 5 °C with magnetic stirring. Initially, 89 mL of deionized water was added to the reaction vessel at 5 °C. Subsequently, 1 mL of $HAuCl_4$ solution [0.1 M] was added. Following this, $NaBH_4$ [0.13 M] (14 mL) was added drop by drop, and the mixture was left to stir under magnetic stirring for 30 min. The solution underwent a color change from colorless to yellow, then to pink, and finally to wine color.

Characterization

All analyses and antibacterial assays were conducted on AuNPs@amox and AuNPs that were washed by dialyzed using a 10 kDa cut-off cellulose membrane against deionized water for 6 h to remove any unreacted chemicals.

The AuNPs@amox and AuNPs shape and size were determined by transmission electron microscopy (TEM, Hitachi 7700). Measurements were performed on 500 particles using ImageJ program. To determine the surface charge, stability (Z-potential), and hydrodynamic size (DLS) of AuNPs@amox at a concentration of 10 µg/mL sterile deionized water, nanoparticles were diluted and suspended in 0.5X Trypticase Soy Broth (TSB). These characteristics were obtained using a Malvern Instrument Nano-S. The surface plasmon resonance shifts of AuNPs@amox and amoxicillin were evaluated by UV–Visible Thermo-Scientific Evolution 220 Spectrophotometer. Amoxicillin and AuNPs@amox were analyzed using Fourier transform infrared spectroscopy (FTIR) with Perkin Elmer infrared spectrometer in absorbance mode. The antibiotic load of the nanoparticles was determined by thermogravimetric analysis (TGA) Q 600 Analyzer from TA Instruments. Samples were heated in

air over a temperature range of 30–900 °C at 10 °C/min. For the functionalization of AuNPs@amox and the type of bond generated, X-ray photoelectron spectroscopy (XPS) was employed, using XPS Escalab 250Xi Thermofisher.

Antibacterial essays

The strains selected for the investigation were methicillin-resistant *S. aureus* (MRSA) and multi-resistant *A. baumannii.*

The treatments were generated in sterile Corning vials. First, 0.5X TSB was added. Then a concentration of 1×10^8 UFC/mL or 0.1 OD at 600 nm was used, along with amoxicillin at 27.5 µg/mL. AuNPs@amox and AuNPs at 0.1, 0.3, 0.5, and 10 µg/mL were added, and the remaining volume was filled with sterile distilled water to reach a total volume of 6 mL. Subsequently, they were incubated at 37 °C for 24 h under orbital shaking at 150 rpm in MaxQ 4450, Thermo Fisher Scientific incubator.

After incubation, a 100 µL aliquot was taken, and a 1:10 serial dilution (bacterial culture: PBS) was performed. It was seeded on TSB agar Petri dish using the microdrop technique described by Miles et al., with triplicate aliquots of 10 µL taken for each dilution.

To assess cell wall damage, the bacteria were observed using scanning electron microscopy (SEM, Hitachi SU3500). The sample preparation method, as modified by Ulloa-Ogaz et al., was employed [44].

Assay for biofilm formation

The quantitative method for testing biofilm formation, as described by Stepanović et al., [45] was applied. A 12-h pre-inoculum of MRSA and *A. baumannii* was used. Treatments were prepared and then adjusted in PBS solution at 1×10^8 UFC/mL. The treatments included a negative control (TSB), bacteria, a positive control (amoxicillin and AuNPs), and AuNPs@amox). Subsequently, they were incubated at 37 °C for 24 h under orbital shaking at 150 rpm using a MaxQ 4450, Thermo Fisher Scientific.

In a 96-well plate, a 200 µL aliquot of each treatment in triplicate was adjusted to an OD of 0.1 in PBS, along with the negative control. Additionally, the plate was covered and left to incubate while shaking at 150 rpm for 24 h at 37 °C. The excess broth was carefully removed from each well and washed thrice with 250 µL of PBS. The plates were shaken between each wash to remove bacteria that did not adhere to the wells. Afterward, they were fixed with 200 µL of 99.9% methanol in each well and incubated at 4 °C for 10 min. After incubation, the excess alcohol was removed, and the wells were dried. Subsequently, the wells were stained with 200 µL of 2% Hucker's crystal violet for 5 min. Excesses stain was rinsed with sterile distilled water, and the wells were dried. The absorbance was measured at 570 nm in triplicate using VarioScan-Lux with SkanIt Software 4.1 for Microplate Readers RE.

The percentage of biofilm was determined with the following equation:

$$\%Biofilm = \left(\mathrm{OD}\frac{\text{sample}}{\mathrm{OD}}\text{negative control}\right)\times 100 \quad (1)$$

Statistical analysis

A one-way ANOVA statistical analysis of variance was performed, complying with Kolmogorov-Smirnoff normality and homogeneity of variances with the Levene test ($\alpha=0.05$). Grouping was performed using the Tukey where groups sharing the same letter do not have significant differences. The analyses were carried out in STADISTICS 7 and plotted in Origin Pro 2022.

Results and discussion

Synthesis and characterization of gold nanoparticles

AuNPs control micrographs display monodisperses spherical-shaped with a size 4 ± 1.8 nm (Fig. 1a). Similarly, in the synthesis of AuNPs@amox, by modifying the reaction time and temperature, it was possible to achieve a pH 7, favoring control over size dispersion and morphology of AuNPs [46]. Several authors have reported that AuNPs with spherical and quasi-sphere shapes tend to exhibit low cytotoxicity. However, the antibacterial properties are also dependent on the size of the AuNPs [11]. A size around 5 nm provides a better bacterial interaction between nanomaterial and microorganisms.

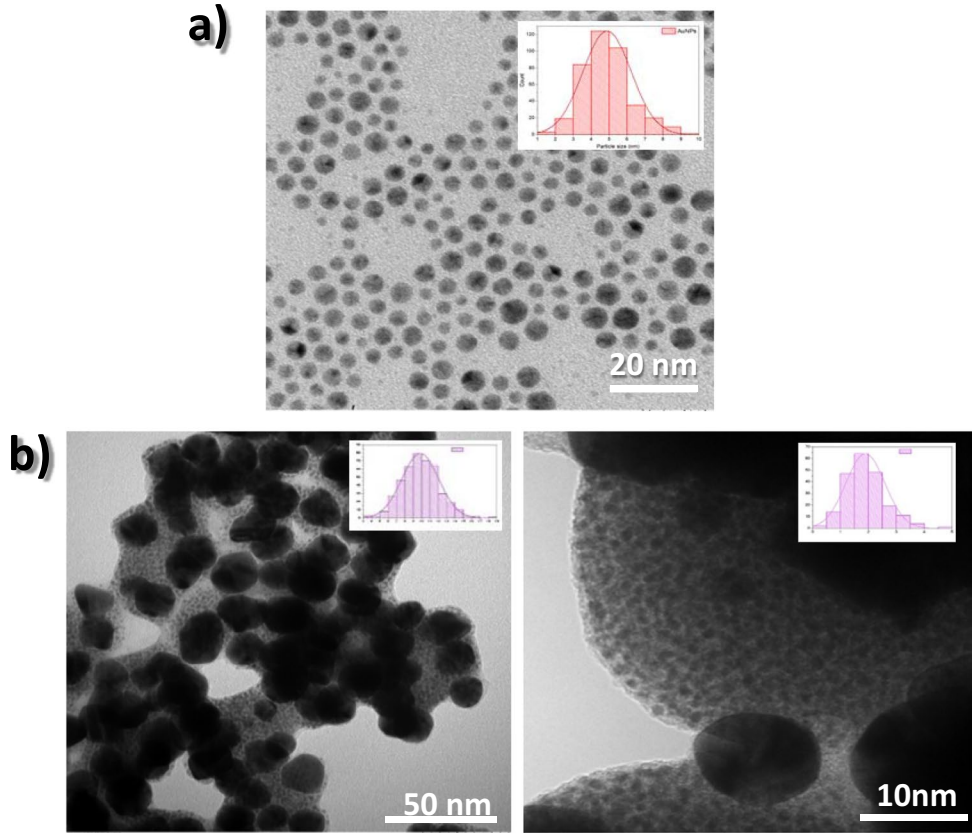

Fig. 1 Morphology and distribution size of **a**) AuNPs control, **b**) AuNPs@amox (low and high magnification)

The TEM images of AuNPs@amox depict quasi-sphere shape and a bimodal size ranging between 9 ± 2, and 1 ± 0.6 nm (Fig. 1b). Through adjustments in reaction time and temperature, we successfully controlled the pH of the solution (6.98), resulting in smaller AuNPs@amox compared to those reported by Demurtas et al. They obtained Amox-GNPs sized at 32.61 ± 4.78 nm and 2 nm, attributing this effect to the reduction of Au by the amino groups present in amoxicillin. This phenomenon was confirmed as the nucleation of the particles rapidly decreased due to the neutralization of the solution.

The AuNPs and AuNPs@amox exhibited colloidal stability, with negative surface charges of -25 mV and -14.1 mV respectively. This reduction suggests that amoxicillin, with its positive charge, establishes a strong interaction or bond with AuNPs, leading to a decrease in the *Z*-potential value of AuNPs. Similar effects have been reported in functionalization of MNPs with various antibiotics [19, 20, 27, 28]. These alterations may indicate that attractive forces, including hydrogen bonds, play a crucial role in facilitating the drug-loading process. DLS analysis revealed an increase in the hydrodynamic size from 120 ± 15 to 138 ± 10 nm for AuNPs and AuNPs@amox respectively. The presence of TSB can induce agglomeration in AuNPs@amox and AuNPs agglomeration, owing to its varying concentration of sugars, proteins, inorganic salts, and other compounds, resulting in a high ionic strength. This phenomenon can influence the physicochemical properties of the MNPs, such as hydrodynamic size, ion release, stability, and surface charge [29].

The absorbance of amoxicillin, AuNPs, and AuNPs@amox by UV–Vis analysis is shown in Fig. 2A. The analysis revealed a maximum peak at 515 nm for AuNPs, while amoxicillin exhibited its maximum peak at 270 nm. While AuNPs@amox first peak is close to 265 nm, a second peak is observed

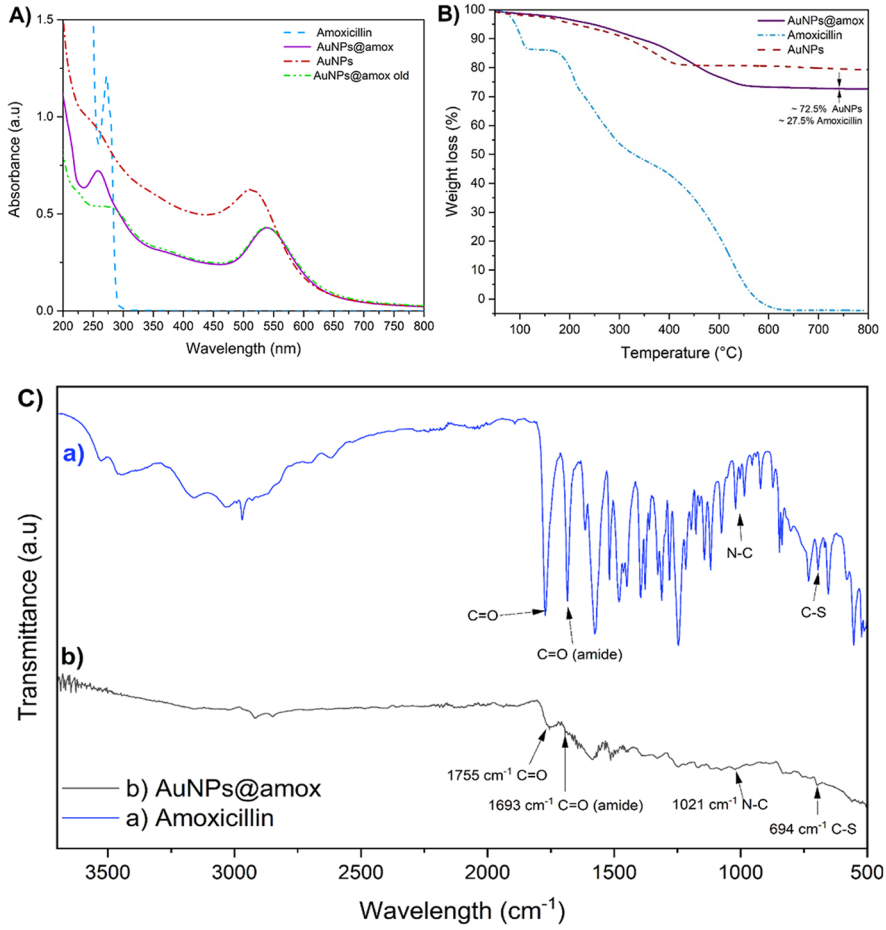

Fig. 2 Evaluation of the presence of amoxicillin in the gold nanoparticle surface. **A**) UV–Vis spectra of gold nanoparticles functionalized with (a) amoxicillin (purple continue line), (b) AuNPs (red), and (c) amoxicillin (light blue dots line). **B**) TGA analysis amoxicillin (blue dots line), AuNPs (red discontinue line), and gold nanoparticles functionalized with amoxicillin (purple continue line). **C**) FTIR spectra of (a) amoxicillin and (b) gold nanoparticles functionalized with amoxicillin shown the principal bands of β-lactam ring

around 545 nm, indicating a shift towards the infrared (bathochromic shift).

This shift could be attributed, to the presence of the protonated nitrogen atom in the amoxicillin molecule and the interaction of the positively charged amine group on the surface of the AuNPs. Moreover, the red shift also suggests an increase in the particle size, possibly indicating the bonding of the amino group, where organic protection increases the size of the nanoparticle. On the other hand, the bandwidth indicates a narrow distribution of sizes and morphologies for AuNPs@amox, suggesting a low variation of sizes and morphologies, as observed in Fig. 1a, and b.

The stability of AuNPs@amox after 1 year of synthesis is demonstrated in Fig. 2A, which shows the analysis of amoxicillin over time. UV–Vis analysis reveals a peak at 270-nm wavelength, characteristic of amoxicillin regardless of the time elapsed since synthesis. Both the newly synthesized nanoparticles and those stored for a year show the same peak at 280 nm, with a slight bathochromic shift towards the infrared region. This shift is attributed to the acidification of the medium, as the nanoparticles are suspended in water. However, there is a loss of amoxicillin of approximately 8.5% within 1 year of synthesis when suspended in water. The behavior observed in the thermogram indicates acidification of the sample, which leads to the disruption of electrostatic formed between the AuNPs and amoxicillin.

Through TGA analysis (Fig. 2B), the content of Au was determined based on the decomposition of organic substances, specifically at 750 °C [47]. The thermal stability below 150 °C, exhibited by AuNPs@amox, results in a weight loss close to 3%. Then, the thermograms differ because they contain different organic coatings. Regarding the thermogram of amoxicillin, it undergoes a total degradation below

650 °C. As a result, AuNPs@amox exhibits an amoxicillin close to 27.5% determined, while the AuNPs residual content is 72.5%. AuNPs and amoxicillin have a percentage of 69% and 31%, respectively, according to the synthesis conditions. This amoxicillin loading has a reductive ability towards Au^{+3} ions; the electrostatic functionalization involves chemisorption of organic units on the surface of the nanoparticle (in this case amine groups). Due to the electronegativity of such units, the surface of the nanoparticle becomes charged. And due to this charge (either negative), particles push each other, as observed in the *Z*-potential analysis. This phenomenon could be the electrostatic stability. Previous investigations by Demurtas et al., Silvero et al., and Chavan et al., [22, 25, 31] reported 33%, 11%, and 30%, respectively, of antibiotic loading on the surface of nanoparticles.

FTIR analysis shows the presence of amoxicillin on the surface of AuNPs (Fig. 2C); it is possible to observe characteristic bands of the β-lactam ring [48, 49] around 1755 cm^{-1}, the stretching C = O bond, and at 1693 cm^{-1}, the stretching C = O bond of the amide group was located. Also, the stretching of N–C of β-lactam was detected at 1021 cm^{-1}. The bending C–S of the thiazole ring was detected at 694 cm^{-1}. It is essential not to damage the ring, to avoid losing the reactive site of the antibiotic. The presence of these groups coincides with the signals presented by amoxicillin; therefore, it can be deduced that the AuNPs are functionalized with amoxicillin.

The research carried out by Rogowska et al., Kalita et al., Silvero et al., and Demurtas et al. suggests that the functionalization of MNP's by electrostatic bonds with the amino group of the amoxicillin or ampicillin molecule occurs due to the high electronic affinity presented by nitrogen with metal, such as gold or silver, and atoms [50]. However, different authors have shown that gold has a low cytotoxicity, unlike silver, which can cause cytotoxicity. The presence of gold and sulfur is corroborated by elemental mapping (Fig. S1) and XPS analysis.

In the XPS analysis of AuNPs@amox for Au (Fig. 3a), the spectrum exhibits three components representative of metallic Au. The component with the highest intensity is attributed to Au^0, with its doublet $4f_{7/2,5/2}$ at 82.68 eV. The component with medium intensity is attributed to Au^{+1}, with its doublet at 84.09 eV. The component with the lowest intensity corresponds to Au^{+3}, with its $4f_{7/2}$ at 88.2 eV. These components are indicative of changes in the oxidation states of Au during the synthesis.

In the oxygen spectrum of AuNPs@amox (Fig. 3b), two O 1 s components are maintained at a lower intensity, preserving the active site of the antibiotic at 531.93 eV and attributed to the O = C–N bond. However, in the amoxicillin spectra (Fig. 3c), two main components can be observed in the O 1 s orbital. The higher intensity peak at 531.68 eV is attributed to the O = C–N covalent bond, referring to the β-lactam ring. Meanwhile, the lower intensity O 1 s component at 533.23 eV corresponds to the C–OH bonds present in the antibiotic molecule.

In the spectrum of Fig. 3d for AuNPs@amox, only one component was found at the binding energy for the N 1 s at 399.7 eV, which corresponds to the amide group (N–C = O) present in the amoxicillin molecule according to the NIST database. Meanwhile, in the representative spectrum of amoxicillin (Fig. 3e), for the N 1 s, two components were found. The higher intensity component located at 400.01 eV is attributed to the N–C = O bond (amide), while, the lower intensity component was located at 401.06 eV corresponds ($C–NH_2$). The analysis for AuNPs@amox is that a shift to a lower intensity of this same component was found, placing the S $2p_{3/2}$ at 169.15 eV (Fig. 3f); generally, this binding energy is associated with oxidized sulfur species (S = O sulfones) [51]. However, since the O 1 s peak (Fig. 3b) is not present at 533.5 eV, so, we cannot confirm the oxidation of the S, whereas Fig. 4g presents the spectrum of the S of amoxicillin, which fitted an S $2p_{3/2}$ component at 163.40 eV with one doublet located at 165.38 eV, attributed to the C–S–C bond present in the antibiotic.

In the absence of binding energy peak at 529 eV in the oxygen spectrum, it was confirmed that this is not an oxidation of Au, but rather an incomplete reduction of Au [52]. Additionally, since there is no binding energy peak at 90.8 eV in the AuNPs@amox spectrum, an Au–S covalent bond can be ruled out. In the observed Au spectrum for AuNPs@amox functionalization through covalent Au–S bond is also ruled out, as no such interaction is present at a BE = 162 eV in the S $2p_{3/2}$. Therefore, since the amino group bond is not present in the spectrum of AuNPs@amox (Fig. 3d), the possible electrostatic N–Au functionalization is deduced. This loss of component phenomenon in a functionalized material has been reported previously by Silva et al. [53], in their

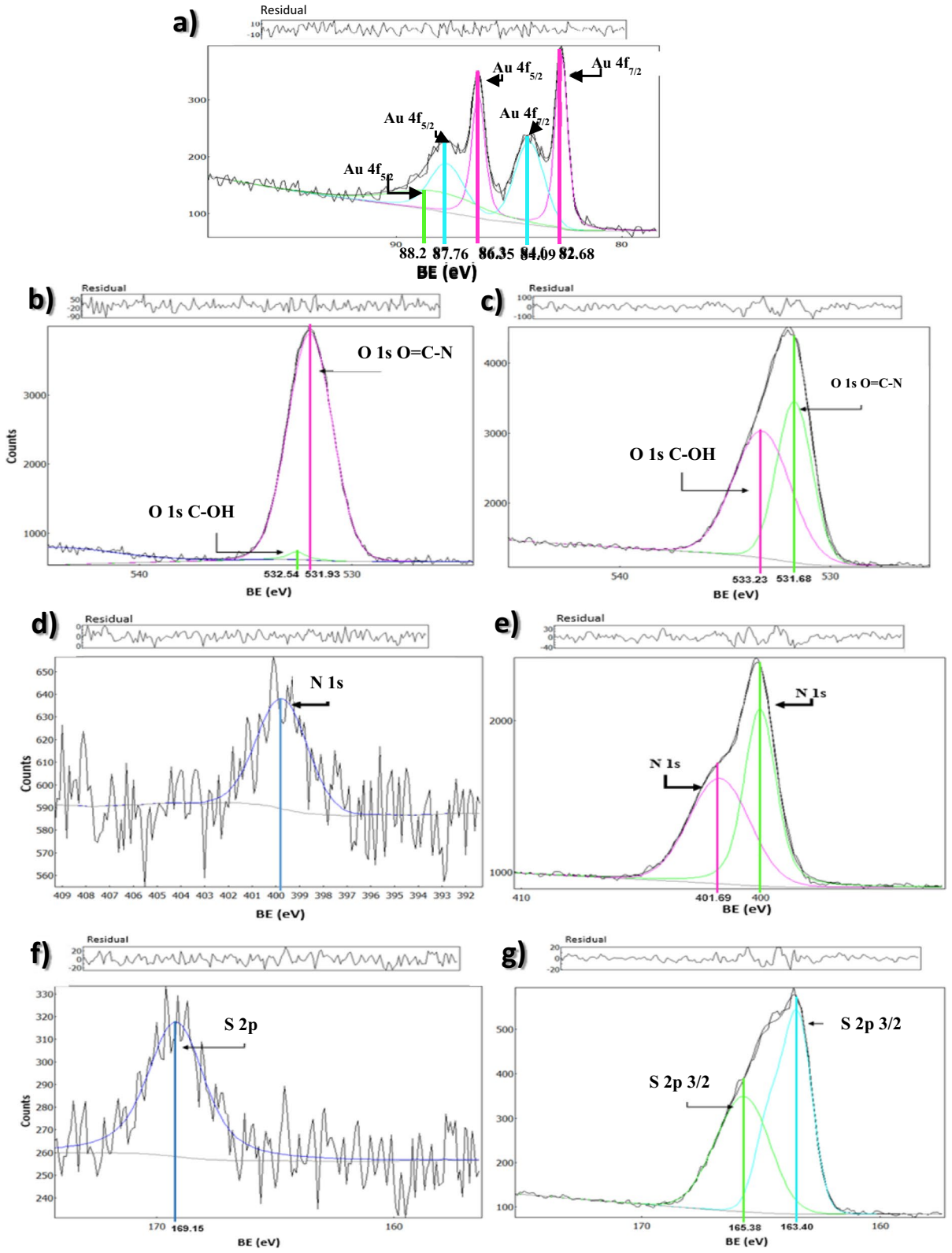
a)
Residual
Au 4f5/2
Au 4f7/2
Au 4f5/2
Au 4f7/2
Au 4f5/2
88.2 87.76 86.35 84.09 82.68
BE (eV)
b)
Residual
O 1s O=C-N
O 1s C-OH
Counts
532.54 531.93 530
BE (eV)
c)
Residual
O 1s O=C-N
O 1s C-OH
533.23 531.68 530
BE (eV)
d)
Residual
N 1s
Counts
BE (eV)
e)
Residual
N 1s
N 1s
401.69 400
BE (eV)
f)
Residual
S 2p
Counts
169.15
BE (eV)
g)
Residual
S 2p 3/2
S 2p 3/2
165.38 163.40
BE (eV)

◂**Fig. 3** X-ray photoelectron spectra. **a**) Au 4f analysis of AuNPs@amox. **b**) O 1 s components of AuNPs@amox. **c**) Components O 1 s of amoxicillin. **d**) Component N 1 s of AuNPs@amox. **e**) Components N 1 s of amoxicillin. **f**) S 2p analysis of AuNPs@amox. **g**) S 2p analysis of amoxicillin

investigation where they coated biomedical textiles with chitosan-functionalized AuNPs. They demonstrated a possible interaction of Au^0 with the amino group of chitosan (NH_2) forming a weak electrostatic bond with the negatively charged nanoparticle.

Antibacterial properties

The AuNPs@amox exhibited the ability to inhibit MRSA by 76 to 80% as shown in Fig. 4. The highest level of inhibition achieved is 80.41%, attributed to a concentration of 10 µg/mL. However, assays did not reveal significant differences between concentrations AuNPs@amox. In *A. baumannii*, the response of the bacteria to AuNPs@amox was different. The assays indicated that as the concentration increased, the percentage of inhibition decreased from 76 to 60%, showing significant differences. The concentration of 0.1 µg/mL yielded the highest inhibition percentage (76.95%). While at 10 µg/mL of AuNPs@amox, the percentage inhibition decreases to 60.18%. This could be attributed to possible agglomeration or precipitation of the AuNPs@amox, caused by the bacteria biofilm or trypticase soy broth (TSB) [42]. AuNPs with 4 nm exhibit considerable antimicrobial properties, inhibiting MRSA by 33.85 to 39.31% at concentrations of 0.1, 0.3, 0.5, and 10 µg/mL, without significant differences. Nevertheless, as the concentration of AuNPs increased, the percentage of inhibition decreased. In contrast, the behavior was different in *A. baumannii*, generating significant differences between the distinct concentrations. The percentage of inhibition ranges between 24.59 and 56.3%.

The damage caused to MRSA is displayed in Fig. 5, where the bacteria exposed to amoxicillin show no observed damage. However, cell wall damage becomes evident when the cells are exposed to distinct concentrations of AuNPs and AuNPs@amox. Initially, the bacteria generated a biofilm, hollows, and flattening. Yet, when in the presence of AuNPs and AuNPs@amox, this biofilm is damaged, with observable gaps and strands. The cell wall damage is also evident at concentrations of 0.5 µg/mL, where more significant cell death was detected compared to the concentrations 0.1 or 0.3 µg/mL. Even more, when the cells were exposed to AuNPs at 10 µg/mL, they exhibited crushing, perforations in their membranes, and a reduction in cell size. Nevertheless, when MRSA was exposed to AuNPs@amox, a complete change in cell morphology from cocci to bacilli was observed. These cells exhibited several perforations in their structure, leading to cell lysis.

The A. baumannii micrograph shows no damaged cells in bacteria control and the presence of amoxicillin (Fig. 6). Cell damage in all the AuNPs and AuNPs@amox is characterized by perforations, holes, and shrinkage. Additionally, changes in the morphology and dimensions of the cell width were observed, reducing from 0.5–1 µm to values no greater than 0.5 µm, resembling cells with the appearance of small coco-bacilli. As the concentration increased to 10 µg/mL, it was observed that the bacteria were unable to undergo cell division, resulting in the generation of elongated cells. Upon exposure to AuNPs@amox at 10 µg/mL, the cells exhibited holes, and their lengths were larger than those in the bacteria control but smaller than in the presence of AuNPs.

Since the bacterial cell wall is a key component of bacteria, its main function is to maintain the cell shape and allow the cell to resist osmotic pressure, as well as to protect the peptidoglycan layer. In Gram-positive bacteria, peptidoglycan constitutes the major part of the coat and provides structural stability to the cell wall [54–56]. The morphological change from cocci to bacilli that MRSA underwent at 10 µg/mL AuNPs@amox (Fig. 5j) may be due to the synergy between the mechanisms of action of the NPs and amoxicillin, as well as the bimodal behavior obtained in the NPs. It has been reported that the NPs may interact with the cell wall by altering the cross-linking of the enzymes responsible for generating peptidoglycan. Interaction with the cell surface and internalization into the cytoplasm are easier for NPs with smaller sizes due to fewer spatial obstacles [57–59].

In turn, the AuNPs have amoxicillin on their surface, which is a β-lactam antibiotic. Its main function is to bind to specific PBPs in the bacterial cell wall and inhibit the assembly of peptidoglycan chains [60]. The local stress induced by NPs, in this case, AuNPs@amox on bacterial membranes, causes membrane rupture. This could be a factor contributing to a considerable antibacterial effect, primarily through

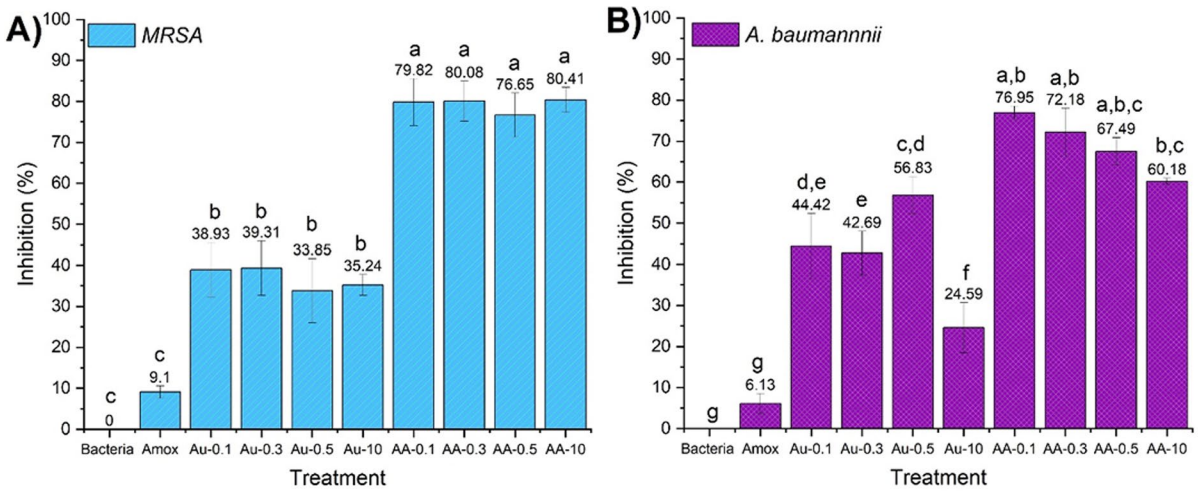

Fig. 4 Antibacterial activity of AuNPs@amox in clinical isolates after 24-h incubation at 37 °C. **A**) Methicillin-resistant *Staphylococcus aureus* (MRSA), and **B**) *Acinetobacter baumannii* resistant to multiple antibiotics. Different literals represent statistically significant differences ($p < 0.05$). Amox, Amoxicillin; AA-x, AuNPs@amox at 0.1/0.3/0.5/10 µg/mL

electrostatic interaction between bacterial membranes and AuNPs due to opposite surface charges [54, 61], as well as the AuNPs@amox were able to damage the efflux pumps (Fig S2) promoting cell death.

It has been studied that there is a difference between the *Z*-potential of bacteria and NPs. Generally, bacteria will have Z-potential of around − 26 mV and NPs around − 10 to − 15 mV [62]. In this case, AuNPs@amox, the *Z*-potential was − 14.1 mV. This potential difference implies an attractive force between the pathogen and the NPs. The outer envelope responds to the stress created by making the cell membrane of the bacteria positive. If the NPs are administered above minimal levels, they can create a charge difference sufficient to aggregate the NPs to the surface of the bacteria [63, 64].

Figure 7 displays one of the main resistance mechanisms of MRSA and *A. baumannii* biofilm production. It was found that MRSA generates 130.5% of biofilm, while *A. baumannii* generates 144.95%. However, when both bacteria were exposed to AuNPs and AuNPs@amox at concentrations of 0.1, 0.3, and 0.5 µg/mL, biofilm production increased. Despite the high biofilm production of MRSA, when the concentration of AuNPs and AuNPs@amox is increased to 10 µg/mL, the biofilm significantly decreased by up to 80% in the presence of AuNPs, resulting in low biofilm production with slight adherence. When subjected to AuNPs@amox, it could be reduced by up to 65%, with no adherence compared to the control.

Biofilm production is a crucial factor in the pathogenesis, antibiotic resistance, and immune evasion of bacteria. Yang et al., [65] found that *A. baumannii* tends to increase biofilm formation when exposed to antibiotics such as amoxicillin. They determined that this might be attributed to the stress induced by the antibiotic, which enhances gene regulation and provides fitness advantages for resistant strains.

Chavan et al. [26] reported the use of ampicillin as a reducing and protecting agent to form ampicillin-coated gold nanoparticles (Amp-Au NPs). Amp-Au NP exhibited antimicrobial activity against resistant bacteria, with up to a 16-fold and fourfold increase in effectiveness, respectively. In a study by Demurtas et al. [43], amoxicillin-loaded gold nanoparticles were synthesized. The research reported that 33 µg/mL of amoxicillin associated with the gold nanoparticles was sufficient to inhibit the growth of Gram-negative bacteria. Wang et al. [66], vancomycin was employed as a reducing and protecting agent to obtain polygonal-shaped AuNPs. The vancomycin conjugate retained its antibacterial activity, and the conjugate demonstrated a 16-fold reduction in the amount of antibiotic required to inhibit certain vancomycin-resistant enterococci (VRE) strains compared to free-form vancomycin.

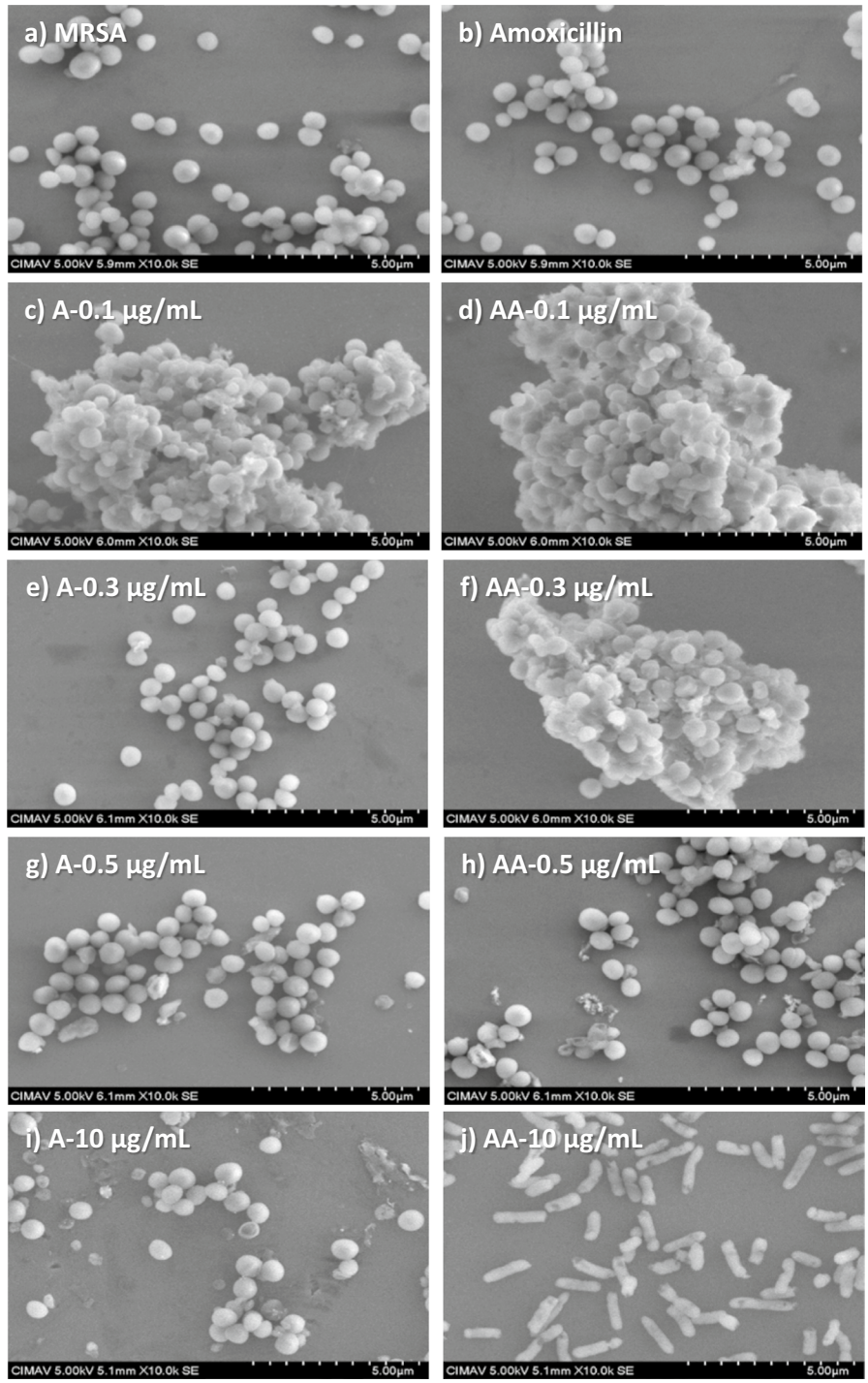

Fig. 5 Cell damage demonstration in methicillin-resistant *Staphylococcus aureus*. **a**) Bacteria control. **b**) Amoxicillin control. **c**) AuNPs at 0.1 µg/mL. **d**) AuNPs@amox at 0.1 µg/mL. **e**) AuNPs at 0.3 µg/mL. **f**) AuNPs@amox at 0.3 µg/mL. **g**) AuNPs at 0.5 µg/mL. **h**) AuNPs@amox at 0.5 µg/mL. **i**) AuNPs at 10 µg/mL. **j**) AuNPs@amox at 10 µg/mL

Brown et al., [33] used ampicillin alone against both gram-positive and negative strains, finding them to be resistant. However, when they utilized AuNPs conjugated with ampicillin, they discovered a malfunction in the efflux system due to the blocking effect of the gold nanoparticles. Additionally, they noted multivalent targeting of the drug to the pathogen. These AuNPs were also observed to alter the

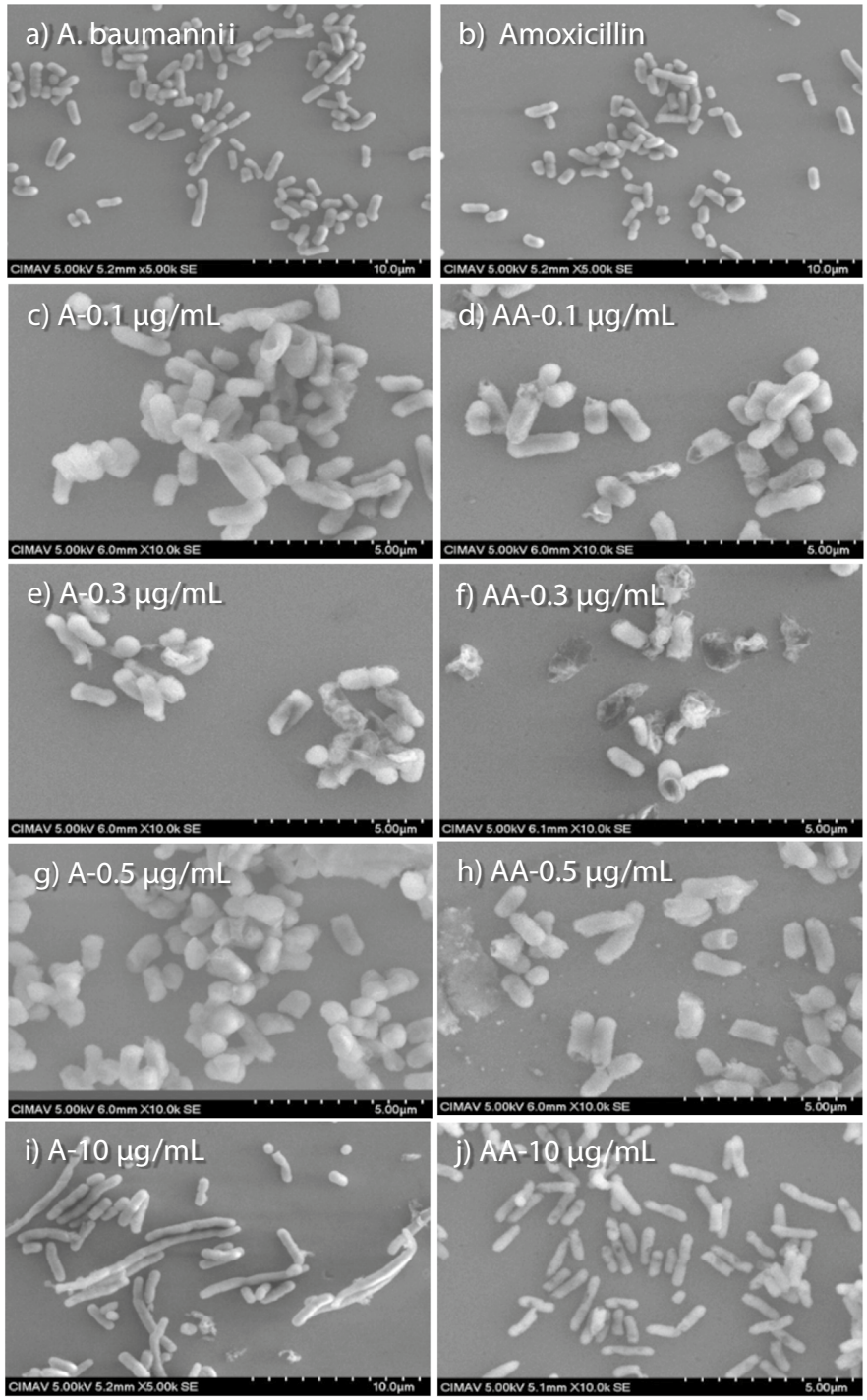

Fig. 6 Cell damage demonstration in multi-resistant *Acinetobacter baumannii*. **a**) Bacteria control. **b**) Amoxicillin control. **c**) AuNPs at 0.1 µg/mL. **d**) AuNPs@amox at 0.1 µg/mL. **e**) AuNPs at 0.3 µg/mL. **f**) AuNPs@amox at 0.3 µg/mL. **g**) AuNPs at 0.5 µg/mL. **h**) AuNPs@amox at 0.5 µg/mL. **i**) AuNPs at 10 µg/mL. **j**) AuNPs@amox at 10 µg/mL

tRNA of the translation pathway, preventing it from binding to the required subunit and consequently disrupting the entire protein configuration. In a similar study, Khameneh et al.[67] confirmed findings similar to those of Gu et al., [68] investigated the mechanism of action of vancomycin-conjugated AuNPs revealing a multivalent inhibition of efflux pumps against *Enterococcus*. Likewise, Mohamed et al., [25] reported

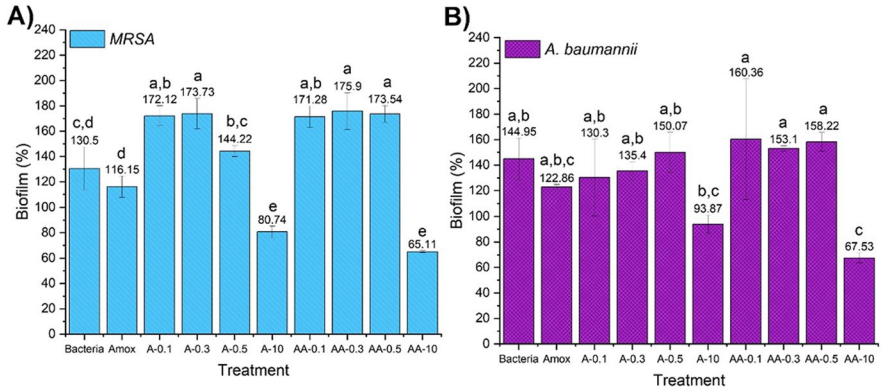

Fig. 7 Biofilm production from clinical isolates after 24-h incubation at 37 °C in the presence of AuNPs@amox. **A**) Methicillin-resistant *Staphylococcus aureus* (MRSA) and **B**) *Acinetobacter baumannii*-resistant to multiple antibiotics. Different literals represent statistically significant differences ($p < 0.05$). Amox, amoxicillin; A–x, AA-x, AuNPs@amox at 0.1/0.3/0.5/10 µg/mL

that treating *Corynebacterium* with AuNPs resulted in the creation of perforations in the cell wall of the pathogen. Subsequently, these nanoparticles accumulated in the intracellular space, causing additional damage to the efflux pump.

Conclusion

The functionalization of AuNPs with amoxicillin is demonstrated, involving the formation of electrostatic bonds through sulfur and nitrogen elements present in the antibiotic molecule. Significant damage was observed in MRSA and *A. baumannii* with varying concentrations of AuNPs@amox. Specifically, at a concentration of 10 µg/mL, the AuNPs@amox inhibit 80.41% of MRSA, while at a lower concentration of 0.1 µg/mL, it inhibited 76.95% of *A. baumannii*.

The bimodal behavior, coupled with an antibiotic loading of 27.5% proved sufficient to inhibit resistant strains. Enhancing the antimicrobial activity of amoxicillin through the combination appears to be a viable approach in the addressing of antimicrobial resistance. This study demonstrated an alternative route pathway for combinatorial therapy against high drug-resistance by bacteria. The size of AuNPs@amox and AuNPs played a crucial role, potentially hindering the outflow of nanoparticles. Furthermore, the particle size influenced the efflux kinetics of membrane pumps, leading to perforation of cell walls, reduction of biofilms, and ultimately causing cell death.

Acknowledgements A.S.B.G acknowledges Consejo Nacional Humanidades Ciencia y Tecnología her Ph.D. scholarship, Centro de Investigación en Materiales Avanzados and Universidad Autónoma de Chihuahua for their supporting this research, as well as, Hospital Central Universitario de Chihuahua by donated the bacteria. We would like to give special thanks for the technical assistance: Luis De La Torre, Andrés González Jacquez, M.C Raúl Ochoa, M.C Karla Campos, M.C Lilia Bautista, M.C Gerardo Silva, PhD. Servando Aguirre, PhD. Alejandro Vega, PhD. Claudia Hernández, PhD. Erasmo Orrantia, PhD. Manuel Roman, and PhD. Daniel Lardizabal.

Author contribution A.S.B-G was responsible for conceptualization, performing, and designing the experiments, original draft preparation, analyzing the data, writing the paper, and editing. H.A.P–C and H.E.E-P of the conceptualization, original draft preparation, writing the paper, editing, resources, materials, and supervision of the process. C.A.R-V and R.R.M of the review, resources and materials, and editing.

Data and code availability Data will be made available on request.

Declarations

Ethical approval Not applicable.

Competing interests The authors declare no competing interests.

References

1. Bullington W, Hempstead S, Smyth AR et al (2020) Antimicrobial resistance: concerns of healthcare providers and

people with CF. J Cyst Fibros. https://doi.org/10.1016/j.jcf.2020.05.009
2. De Oliveira DMP, Forde BM, Kidd TJ et al (2020) Antimicrobial resistance in bacteria. Open Med 4:141–155. https://doi.org/10.2478/s11536-008-0088-9
3. De Oliveira DMP, Forde BM, Kidd TJ et al (2020) Antimicrobial resistance in ESKAPE pathogens. Clin Microbiol Rev 33(3):1–49. https://doi.org/10.1128/CMR.00181-19
4. WHO (2021) Antimicrobial resistance. In: World Heal. Organ. https://www.who.int/news-room/fact-sheets/detail/antimicrobial-resistance. Accessed 13 June 2024
5. Walsh TR, Gales AC, Laxminarayan R, Dodd PC (2023) Antimicrobial resistance: addressing a global threat to humanity. PLOS Med 20:e1004264. https://doi.org/10.1371/journal.pmed.1004264
6. Werth BJ (2020) Overview of antibiotics. In: PharmD, Univ. Washingt. Sch. Pharm. https://www.msdmanuals.com/home/infections/antibiotics/overview-of-antibiotics. Accessed 13 June 2024
7. Nas F (2017) Mechanisms of bacterial antibiotics resistance: a review. J Adv Microbiol 7:1–6. https://doi.org/10.9734/JAMB/2017/37689
8. Reygaert CW (2018) An overview of the antimicrobial resistance mechanisms of bacteria. AIMS Microbiol 4:482–501. https://doi.org/10.3934/microbiol.2018.3.482
9. Santajit S, Indrawattana N (2016) Mechanisms of antimicrobial resistance in ESKAPE pathogens. Biomed Res Int 2016:1–8. https://doi.org/10.1155/2016/2475067
10 Kwon YH (2016) Amoxicillin. Helicobacter pylori. Springer Singapore, Singapore, pp 387–396
11. Sani A, Cao C, Cui D (2021) Toxicity of gold nanoparticles (AuNPs): a review. Biochem Biophys Reports 26:100991. https://doi.org/10.1016/j.bbrep.2021.100991
12. Bayda S, Adeel M, Tuccinardi T et al (2020) The history of nanoscience and nanotechnology: from chemical-physical applications to nanomedicine. Molecules 25:112. https://doi.org/10.3390/molecules25010112
13. Eleraky NE, Allam A, Hassan SB, Omar MM (2020) Nanomedicine fight against antibacterial resistance: an overview of the recent pharmaceutical innovations. Pharmaceutics 12:142. https://doi.org/10.3390/pharmaceutics12020142
14. Kamat S, Kumari M (2023) Emergence of microbial resistance against nanoparticles: mechanisms and strategies. Front Microbiol 14:1102615. https://doi.org/10.3389/fmicb.2023.1102615
15. Balderrama-González A-S, Piñón-Castillo H-A, Ramírez-Valdespino C-A et al (2021) Antimicrobial resistance and inorganic nanoparticles. Int J Mol Sci 22:12890. https://doi.org/10.3390/ijms222312890
16. Patil T, Gambhir R, Vibhute A, Tiwari AP (2023) Gold nanoparticles: synthesis methods, functionalization and biological applications. J Clust Sci 34:705–725. https://doi.org/10.1007/s10876-022-02287-6
17. Xing X, Ma W, Zhao X et al (2018) Interaction between surface charge-modified gold nanoparticles and phospholipid membranes. Langmuir 34:12583–12589. https://doi.org/10.1021/acs.langmuir.8b01700
18. Zuhrotun A, Oktaviani DJ, Hasanah AN (2023) Biosynthesis of gold and silver nanoparticles using phytochemical compounds. Molecules 28:3240. https://doi.org/10.3390/molecules28073240
19. Halawani EMS, Alzahrani SSS, Gad El-Rab SMF (2023) Biosynthesis strategy of gold nanoparticles and biofabrication of a novel amoxicillin gold nanodrug to overcome the resistance of multidrug-resistant bacterial pathogens MRSA and E. coli. Biomimetics 8:452. https://doi.org/10.3390/biomimetics8060452
20. Younis HM, Hussein HA, Khaphi FL, Saeed ZK (2023) Green biosynthesis of silver and gold nanoparticles using Teak (Tectona grandis) leaf extract and its anticancer and antimicrobial activity. Heliyon 9:e21698. https://doi.org/10.1016/j.heliyon.2023.e21698
21. Perveen K, Husain FM, Qais FA et al (2021) Microwave-assisted rapid green synthesis of gold nanoparticles using seed extract of Trachyspermum ammi: ROS mediated biofilm inhibition and anticancer activity. Biomolecules 11:197. https://doi.org/10.3390/biom11020197
22. Soliman MKY, Salem SS, Abu-Elghait M, Azab MS (2023) Biosynthesis of silver and gold nanoparticles and their efficacy towards antibacterial, antibiofilm, cytotoxicity, and antioxidant activities. Appl Biochem Biotechnol 195:1158–1183. https://doi.org/10.1007/s12010-022-04199-7
23. Dehghani F, Mosleh-Shirazi S, Shafiee M et al (2023) Antiviral and antioxidant properties of green synthesized gold nanoparticles using Glaucium flavum leaf extract. Appl Nanosci 13:4395–4405. https://doi.org/10.1007/s13204-022-02705-1
24. Cui Y, Zhao Y, Tian Y et al (2012) The molecular mechanism of action of bactericidal gold nanoparticles on Escherichia coli. Biomaterials 33:2327–2333. https://doi.org/10.1016/j.biomaterials.2011.11.057
25. Mohamed MM, Fouad SA, Elshoky HA et al (2017) Antibacterial effect of gold nanoparticles against Corynebacterium pseudotuberculosis. Int J Vet Sci Med 5:23–29. https://doi.org/10.1016/j.ijvsm.2017.02.003
26. Chavan C, Kamble S, Murthy AVR, Kale SN (2020) Ampicillin-mediated functionalized gold nanoparticles against ampicillin-resistant bacteria: strategy, preparation and interaction studies. Nanotechnology 31:215604. https://doi.org/10.1088/1361-6528/ab72b4
27. Patil T, Khot V, Pandey-Tiwari A (2022) Single-step antibiotic-mediated synthesis of kanamycin-conjugated gold nanoparticles for broad-spectrum antibacterial applications. Lett Appl Microbiol 75:913–923. https://doi.org/10.1111/lam.13764
28. Fan Y, Pauer AC, Gonzales AA, Fenniri H (2019) Enhanced antibiotic activity of ampicillin conjugated to gold nanoparticles on PEGylated rosette nanotubes. Int J Nanomedicine 14:7281–7289. https://doi.org/10.2147/IJN.S209756
29. Silvero CMJ, Rocca DM, de la Villarmois EA et al (2018) Selective photoinduced antibacterial activity of amoxicillin-coated gold nanoparticles: from one-step synthesis to in vivo cytocompatibility. ACS Omega 3:1220–1230. https://doi.org/10.1021/acsomega.7b01779
30. Kalita S, Kandimalla R, Sharma KK et al (2016) Amoxicillin functionalized gold nanoparticles reverts MRSA resistance. Mater Sci Eng C 61:720–727. https://doi.org/10.1016/j.msec.2015.12.078

31. Rad MR, Kazemian H, Yazdani F et al (2019) Antibacterial activity of gold nanoparticles conjugated by aminoglycosides against A. baumannii isolates from burn patients. Recent Pat Antiinfect Drug Discov 13:256–264. https://doi.org/10.2174/1574891X13666180828115543
32. Mohamed MA (2020) Myco-engineered gold nanoparticles from Jahnula aquatica coated with ampicillin/amoxicillin and their antibacterial and anticancer activity against cancer cells. Biotechnol Lett 42:151–170. https://doi.org/10.1007/s10529-019-02764-5
33. Brown AN, Smith K, Samuels TA et al (2012) Nanoparticles functionalized with ampicillin destroy multiple-antibiotic-resistant isolates of Pseudomonas aeruginosa and Enterobacter aerogenes and methicillin-resistant Staphylococcus aureus. Appl Environ Microbiol 78:2768–2774. https://doi.org/10.1128/AEM.06513-11
34. Barabadi H, Jounaki K, Pishgahzadeh E, et al (2022) Antiviral potential of green-synthesized silver nanoparticles. Handbook of Microbial Nanotechnology. Elsevier, p 285–310
35. Mahdi LH, Hasoon BA, Sulaiman GM et al (2024) Antimicrobial efficacy of l-glutaminase (EC 3.5.1.2) against multidrug-resistant Pseudomonas aeruginosa infection. J Antibiot (Tokyo) 77:111–119. https://doi.org/10.1038/s41429-023-00678-z
36. Yosif HM, Hasoon BA, Jabir MS (2023) Laser ablation for synthesis of hydroxyapatite and Au NP conjugated cefuroxime: evaluation of their effects on the biofilm formation of multidrug resistance Klebsiella pneumoniae. Plasmonics. https://doi.org/10.1007/s11468-023-02053-y
37. Singh J, Kumar S, Dhaliwal AS (2020) Controlled release of amoxicillin and antioxidant potential of gold nanoparticles-xanthan gum/poly (Acrylic acid) biodegradable nanocomposite. J Drug Deliv Sci Technol 55:101384. https://doi.org/10.1016/j.jddst.2019.101384
38. Rocca DM, Silvero CMJ, Aiassa V, Cecilia Becerra M (2020) Rapid and effective photodynamic treatment of biofilm infections using low doses of amoxicillin-coated gold nanoparticles. Photodiagnosis Photodyn Ther 31:101811. https://doi.org/10.1016/j.pdpdt.2020.101811
39. Hasoon BA, Jawad KH, Abdulsahib SS (2023) Synthesis of ciprofloxacin-conjugated gold nanoparticles and their study antibacterial effects on growth biofilm formation through nebulizer mask against respiratory infection. Plasmonics. https://doi.org/10.1007/s11468-023-02108-0
40. Giráldez-Pérez RM, Grueso EM, Carbonero A et al (2023) Synergistic antibacterial effects of amoxicillin and gold nanoparticles: a therapeutic option to combat antibiotic resistance. Antibiotics 12:1275. https://doi.org/10.3390/antibiotics12081275
41. Jawad KH, Jamagh FK, Sulaiman GM et al (2024) Antibacterial and antibiofilm activities of amikacin-conjugated gold nanoparticles: a promising formulation for contact lens preservation. Inorg Chem Commun 162:112286. https://doi.org/10.1016/j.inoche.2024.112286
42. Shaikh S, Nazam N, Rizvi SMD et al (2019) Mechanistic insights into the antimicrobial actions of metallic nanoparticles and their implications for multidrug resistance. Int J Mol Sci 20:2468. https://doi.org/10.3390/ijms20102468
43. Demurtas M, Perry CC (2014) Facile one-pot synthesis of amoxicillin-coated gold nanoparticles and their antimicrobial activity. Gold Bull 47:103–107. https://doi.org/10.1007/s13404-013-0129-2
44. Ulloa-Ogaz AL, Piñón-Castillo HA, Muñoz-Castellanos LN et al (2017) Oxidative damage to Pseudomonas aeruginosa ATCC 27833 and Staphylococcus aureus ATCC 24213 induced by CuO-NPs. Environ Sci Pollut Res 24:22048–22060. https://doi.org/10.1007/s11356-017-9718-6
45. Stepanović S, Vuković D, Dakić I et al (2000) A modified microtiter-plate test for quantification of staphylococcal biofilm formation. J Microbiol Methods 40:175–179. https://doi.org/10.1016/S0167-7012(00)00122-6
46. Hu J, Wang Z, Li J (2007) Gold nanoparticles with special shapes: controlled synthesis, surface-enhanced Raman scattering, and the application in biodetection. Sensors 7:3299–3311. https://doi.org/10.3390/s7123299
47. Mistry K, Ibrahim KH, Novodchuk I et al (2020) Nanomechanical gas sensing with laser treated 2D nanomaterials. Adv Mater Technol 5:2000704. https://doi.org/10.1002/admt.202000704
48. Junejo Y, Güner A, Baykal A (2014) Synthesis and characterization of amoxicillin derived silver nanoparticles: its catalytic effect on degradation of some pharmaceutical antibiotics. Appl Surf Sci 317:914–922. https://doi.org/10.1016/j.apsusc.2014.08.133
49. Bebu A, Szabó L, Leopold N et al (2011) IR, Raman, SERS and DFT study of amoxicillin. J Mol Struct 993:52–56. https://doi.org/10.1016/j.molstruc.2010.11.067
50. Saraçoğlu M, Bacınoğlu MB, Mertdinç S, Timur S (2022) Synthesis of sericin coated silver nanoparticles (Ag-Ser) by modified Tollens' method and evaluation of colloidal stability. Appl Phys A 128:424. https://doi.org/10.1007/s00339-022-05568-z
51. Gorup LF, Perlatti B, Kuznetsov A et al (2020) Stability of di-butyl-dichalcogenide-capped gold nanoparticles: experimental data and theoretical insights. RSC Adv 10:6259–6270. https://doi.org/10.1039/C9RA07147D
52. NIST computational chemistry comparison and benchmark database no title. In: NIST Stand. Ref. Database Number 101. https://cccbdb.nist.gov/introx.asp. Accessed 13 June 2024
53. Silva Nascimento L et al (2019) Multifunctional chitosan/gold nanoparticles coatings for biomedical textiles. Nanomaterials 9:1064. https://doi.org/10.3390/nano9081064
54. Willey J, Sherwood L, Woolverton CJ (2017) Prescott's microbiology, 10th. Mc Graw Hill, New York
55. Murray PR, Rosenthal KS, Pfaller MA (2013) Medical microbiology, 9th. Elsevier Inc, EEUU
56. Nikolic P, Mudgil P (2023) The cell wall, cell membrane and virulence factors of Staphylococcus aureus and their role in antibiotic resistance. Microorganisms 11:259. https://doi.org/10.3390/microorganisms11020259
57. Yamamoto O (2001) Influence of particle size on the antibacterial activity of zinc oxide. Int J Inorg Mater 3:643–646. https://doi.org/10.1016/S1466-6049(01)00197-0
58. Mahmoudi M, Sant S, Wang B et al (2011) Superparamagnetic iron oxide nanoparticles (SPIONs): development, surface modification and applications in chemotherapy.

Adv Drug Deliv Rev 63:24–46. https://doi.org/10.1016/j.addr.2010.05.006
59. Matter MT, Li JH, Lese I et al (2020) Multiscale analysis of metal oxide nanoparticles in tissue: insights into biodistribution and biotransformation. Adv Sci 7:1–11. https://doi.org/10.1002/advs.202000912
60. Romaniuk JAH, Cegelski L (2015) Bacterial cell wall composition and the influence of antibiotics by cell-wall and whole-cell NMR. Philos Trans R Soc B Biol Sci 370:20150024. https://doi.org/10.1098/rstb.2015.0024
61. Robinson A, Brzoska AJ, Turner KM et al (2010) Essential biological processes of an emerging pathogen: DNA replication, transcription, and cell division in Acinetobacter spp. Microbiol Mol Biol Rev 74:273–297. https://doi.org/10.1128/MMBR.00048-09
62. Dey N, Kamatchi C, Vickram AS et al (2022) Role of nanomaterials in deactivating multiple drug resistance efflux pumps—a review. Environ Res 204:111968. https://doi.org/10.1016/j.envres.2021.111968
63. Srinivasan R, Santhakumari S, Poonguzhali P et al (2021) Bacterial biofilm inhibition: a focused review on recent therapeutic strategies for combating the biofilm mediated infections. Front Microbiol 12:676458. https://doi.org/10.3389/fmicb.2021.676458
64. Stokes JM, Lopatkin AJ, Lobritz MA, Collins JJ (2019) Bacterial metabolism and antibiotic efficacy. Cell Metab 30:251–259. https://doi.org/10.1016/j.cmet.2019.06.009
65. Yang C-H, Su P-W, Moi S-H, Chuang L-Y (2019) Biofilm formation in acinetobacter baumannii: genotype-phenotype correlation. Molecules 24:1849. https://doi.org/10.3390/molecules24101849
66. Wang S-G, Chen Y-C, Chen Y-C (2018) Antibacterial gold nanoparticle-based photothermal killing of vancomycin-resistant bacteria. Nanomedicine 13:1405–1416. https://doi.org/10.2217/nnm-2017-0380
67. Khameneh B, Diab R, Ghazvini K, Fazly Bazzaz BS (2016) Breakthroughs in bacterial resistance mechanisms and the potential ways to combat them. Microb Pathog 95:32–42. https://doi.org/10.1016/j.micpath.2016.02.009
68. Gu H, Ho P-L, Tsang KWT et al (2003) Using biofunctional magnetic nanoparticles to capture vancomycin-resistant enterococci and other gram-positive bacteria at ultralow concentration. J Am Chem Soc 125:15702–15703. https://doi.org/10.1021/ja0359310